

The energy scale of Dirac electrons in Cd_3As_2

M. Hák,^{1,*} S. Tchoumakov,² I. Crassee,¹ A. Akrap,³ B. A. Piot,¹ C. Faugeras,¹
G. Martinez,¹ A. Nateprov,⁴ E. Arushanov,⁴ F. Teppe,⁵ R. Sankar,^{6,7} Wei-li Lee,⁶
J. Debray,^{8,9} O. Caha,¹⁰ J. Novák,¹⁰ M. O. Goerbig,² M. Potemski,¹ and M. Orlita^{1,11,†}

¹*Laboratoire National des Champs Magnétiques Intenses,*

CNRS-UGA-UPS-INS-EMFL, 25, avenue des Martyrs, 38042 Grenoble, France

²*LPS, Univ. Paris-Sud, Univ. Paris-Saclay, CNRS UMR 8502, 91405 Orsay, France*

³*DQMP, University of Geneva, 1211 Geneva 4, Switzerland*

⁴*Institute of Applied Physics, Academy of Sciences of Moldova, 2028 Chisinau, Moldova*

⁵*Laboratoire Charles Coulomb, CNRS, Université Montpellier, 34095 Montpellier, France*

⁶*Institute of Physics, Academia Sinica, Nankang, 11529 Taipei, Taiwan*

⁷*Center for Condensed Matter Sciences, National Taiwan University, Taipei 10617, Taiwan*

⁸*Université Grenoble Alpes, Institut NEEL, F-38000 Grenoble, France*

⁹*CNRS, Institut NEEL, F-38000 Grenoble, France*

¹⁰*CEITEC MU and Faculty of Science, Masaryk University, 61137 Brno, Czech Republic*

¹¹*Institute of Physics, Charles University, Ke Karlovu 5, 12116 Praha 2, Czech Republic*

(Dated: February 4, 2022)

Cadmium arsenide (Cd_3As_2) has recently become conspicuous in solid-state physics due to several reports proposing that it hosts a pair of symmetry-protected 3D Dirac cones. Despite vast investigations, a solid experimental insight into the band structure of this material is still missing. Here we fill one of the existing gaps in our understanding of Cd_3As_2 , and based on our Landau level spectroscopy study, we provide an estimate for the energy scale of 3D Dirac electrons in this system. We find that the appearance of such charge carriers is limited – contrary to a widespread belief in the solid-state community – to a relatively small energy scale (below 40 meV).

PACS numbers: 78.20.Ls, 71.28.+d, 71.70.Di

I. INTRODUCTION

The presence of three-dimensional (3D) massless Dirac electrons in cadmium arsenide (Cd_3As_2) is nowadays taken as granted, from both experimental and theoretical point of views.^{1–4} Cd_3As_2 is thus often cited as the first identified symmetry-protected 3D Dirac semimetal that is stable under ambient conditions. The cartoon picture of its band structure – with two Dirac cones located along the tetragonal axis – is even viewed as a textbook example for this class of materials.

In reality, the band structure of Cd_3As_2 is far more complex and the presence of Dirac electrons, which are of key interest in this material,¹ is not proven. The broadly extended conical band reported in recent experiments on Cd_3As_2 ^{2–4} is most likely not related to any Dirac physics.^{5,6} Instead, this conical band seems to be a simple consequence of a vanishing band gap in the material studied. The low-energy electronic states – where a pair of truly Dirac cones may indeed be expected^{1,7} – have been so far barely addressed in experiments. Hence, at present, the Dirac electrons in Cd_3As_2 do not represent more than an appealing theoretical construct.

A simplified model of the complex band structure of Cd_3As_2 has been in the past proposed by Bodnar,⁸ who treated this material – in the very first approach – as a conventional narrow-gap Kane semiconductor/semimetal⁹ with a nearly vanishing band gap (E_g). The band structure of Cd_3As_2 thus displays, similar to gapless HgCdTe ,^{10,11} a widely extended conical

band, which is centered around the Γ point (Fig. 1). This cone appears due to the approximate accidental degeneracy of p - and s -like states of arsenic and cadmium, respectively, and is not protected by any symmetry.

A closer look at the band structure of Cd_3As_2 implied by the model of Bodnar also reveals symmetry-protected Dirac cones. These highly-anisotropic and strongly tilted cones appear – or at least, they are theoretically expected – at low energies, around the crossing points of two arsenic-like p -type bands (LH and HH bands in Fig. 1). Such crossing points emerge when the cubic symmetry of a Kane semiconductor/semimetal is reduced to a tetragonal one, which is the case of Cd_3As_2 . The impact of the symmetry lowering on the band structure is quantified by crystal field splitting δ .¹² This parameter describes the energy separation of two p -type bands at $k = 0$ (degenerate in cubic semiconductors¹³) and directly measures the energy scale of Dirac electrons in Cd_3As_2 .

Reliable experimental estimates of the crystal field splitting and band gap parameters – those which are directly determining the shape and scale of Dirac cones in Cd_3As_2 – have been missing so far. In this paper, we examine the Cd_3As_2 bands using Landau level spectroscopy and fill this gap in our understanding of this material. Our results show that cadmium arsenide is a semimetal with a small inverted gap of $E_g = -(70 \pm 20)$ meV, which may host three-dimensional symmetry-protected Dirac electrons, but only at the energy scale not exceeding several dozens of meV.

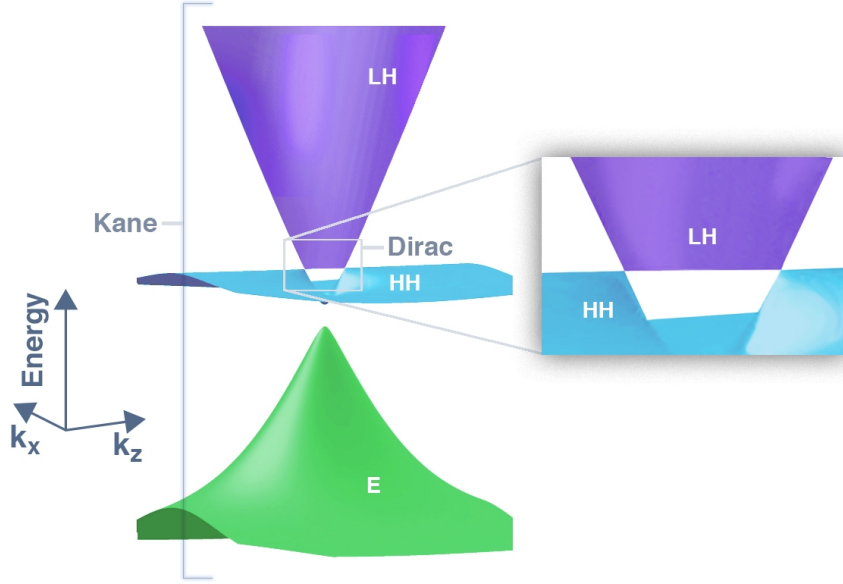


FIG. 1. A schematic view of electronic bands in Cd_3As_2 at the Brillouin zone center. Three electronic bands form two types of 3D conical structures: a single cone hosting Kane electrons at the larger energy scale, appearing due to the vanishing band gap, and two highly tilted and anisotropic 3D Dirac cones at low energies. The Dirac cones emerge at the crossing points of p -type bands, which in semiconductors with non-inverted ordering of bands are referred to as heavy (HH) and light (LH) hole bands¹³. In materials with an inverted band gap (*e.g.*, in HgTe or Cd_3As_2), the LH band becomes the conduction band.

II. EXPERIMENTAL RESULTS AND DISCUSSION

The experiment was performed on a free-standing $80\text{-}\mu\text{m}$ -thick slab of Cd_3As_2 with lateral dimensions of $2 \times 1\text{ mm}^2$, which was grown in a downstream of the tubular furnace from the polycrystalline phase and later detached from the substrate.¹⁴ The x -ray measurements provided us with a diffraction pattern characteristic of Cd_3As_2 ¹⁵ and also showed the existence of a few monocrystalline grains – all with the (112)-orientation, which is the typical growth direction of this material. Similar to other Cd_3As_2 crystals, the sample shows n -type conductivity^{16–19} due to intrinsic defects, with an electron concentration slightly below 10^{19} cm^{-3} .

The studied sample was characterized by zero-field optical spectroscopy in both transmission and reflectivity configurations (Fig. 2a). The reflectivity spectrum, measured using an infrared microscope combined with a conventional Fourier-transform spectrometer, indicates the presence of free charge carriers by a characteristic plasma edge at $\hbar\omega_p \approx 50\text{ meV}$. The fine structure of the plasma edge was also observed in other studies, see, *e.g.*, Refs. 6, 20–22 and it is likely related to non-homogeneous (lateral as well as perpendicular to the surface) distribution of electrons in the explored sample.

The transmission spectrum of the sample shows a well-defined transparency window, which is marked by vertical gray bars in Fig. 2a. At low energies, this transparency window opens just above the plasma edge. At high energies, the transmission window closes due to the onset of interband absorption. The dominant contribu-

tion to this absorption arises from electrons excited from the flat (HH) band to the partially occupied upper conical band,⁶ as schematically shown in the inset of Fig. 2a. The position of the onset of the interband absorption is thus determined by the particular position of the Fermi energy (due to Pauli blocking), which provides us with an estimate of $E_F \approx 160\text{ meV}$. In this estimate we have completely neglected the dispersion of the flat band, which is in reality a hole-like, approximately parabolic band. The corresponding effective mass should be comparable with heavy hole masses in conventional semiconductors¹³ (*i.e.*, approaching the mass of a bare electron in vacuum). The dispersion of this band thus may be neglected in the close vicinity of the Γ point – where the studied (magneto-)optical excitations originate – but has to be considered for momenta comparable with the size of the Brillouin zone, which is the typical scale of ARPES experiments.^{2–4}

The onset of interband excitations may be directly seen in the optical conductivity spectrum (Fig. 2b), which was obtained using the standard Kramers-Kronig analysis of the reflectivity response, complemented by ellipsometry data at high photon energies (inset of Fig. 2b). The smooth spectral profile of this onset indicates a certain spread of the Fermi energy across the probed sample, but likely also some defect/impurity-related absorption within the optical band gap. Above the onset of interband excitations, the optical conductivity follows a linear, or more precisely a weakly superlinear, dependence on the photon energy, which is in perfect agreement with previous studies.^{6,21} The optical conductivity increasing linearly with the photon frequency, $\sigma(\omega) \propto \omega$, is typical

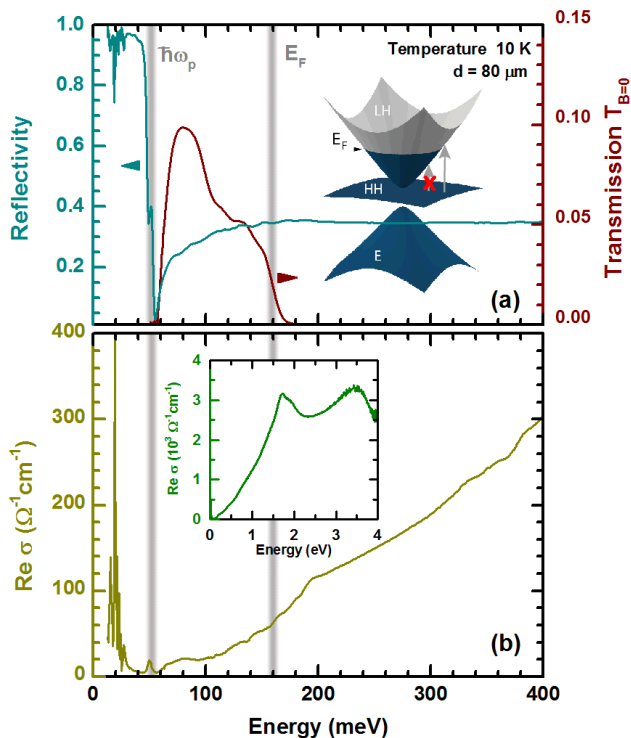


FIG. 2. (a) Transmission and reflectivity spectra of the investigated thin layer of Cd_3As_2 in the far and middle infrared spectral ranges. The upper and lower limits of the transmission window are given by the plasma energy $\hbar\omega_p$ and by the onset of interband absorption, defined by the particular position of the Fermi energy E_F (by Pauli blocking). This is shown in the inset of (a), where the band structure expected within the (gapped) Kane model is schematically plotted. Spectrally sharp features in the reflectivity spectrum visible at low energies are due to infrared active optical phonon modes. The optical conductivity spectrum deduced using Kramers-Kronig relations from the reflectivity curve is plotted in (b). The observed broadening of the onset of interband absorption indicates somewhat inhomogeneous distribution of electrons across the sample, with the mean value of the Fermi energy $E_F \approx 160$ meV. The optical conductivity in a broader spectral range is plotted in the inset of (b).

of systems with 3D massless electrons.^{10,23} The strong increase in the real part of the optical conductivity at low energies is related to intraband (Drude-type, free-carrier) excitations.

The existence of the well-defined transparency window allowed us to probe the response of the sample in magneto-transmission experiments. To perform such measurements, the radiation of a globar was analysed by a Fourier transform spectrometer and using light-pipe optics, delivered to the sample placed in a superconducting coil. The transmitted light was detected by a composite bolometer, placed directly below the sample and kept at the same temperature as the sample (1.8 K). The measurement was done in the Faraday geometry with light propagating perpendicular to the (112) crystal face.

A series of excitations, at energies monotonically increasing with B , is clearly seen in the relative magneto-transmission spectra $T_B/T_{B=0}$ (Fig. 3a) as well as in the false color plot of relative magneto-absorbance $-\ln[T_B/T_{B=0}]$ (Fig. 3a). These excitations appear in the spectra at photon energies significantly higher than the cyclotron energy in the quantum limit, deduced from our preceding high-field magneto-reflectivity experiment.⁶ This points towards the interband origin of these inter-Landau level (inter-LL) excitations.

In the limit of low magnetic fields, these interband resonances seem to asymptotically approach the plasma energy (see color plot in Fig. 3b). This behavior may be viewed as an avoided crossing of interband inter-LL excitations with a plasma resonance, known as the Bernstein modes²⁴. Since the sample is fully opaque at photon frequencies below ω_p , we only observe the upper branch of these coupled modes. Such coupling can be clearly visualized in 2D structures with an additional lateral periodic potential. For instance, such modes have been observed in magneto-optics of quantum wells^{25,26} with the use of surface gratings in order to match inter-LL and plasma frequencies. In 3D samples, such as here, this coupling can be observed more easily since the plasma frequency does not vanish at $\mathbf{q} = 0$ and it was already demonstrated in Raman spectroscopy of n -type GaAs.²⁷ The magneto-optical effects due to this coupling may be richer in systems with a linear dispersion, the gapless character of which implies a series of interband inter-LL excitations at relatively low energies, as discussed in the context of graphene.²⁸ To compare the energy scales of the avoided crossing related to Bernstein modes with the field-induced splitting of the plasma edge expected within the classical theory of magneto-plasma,²⁹ we plotted in Fig. 3b the theoretical positions of the cyclotron resonance active and inactive (CRA and CRI) modes for the corresponding cyclotron mass $m_c = E_F/v^2$.

At high photon energies, well above the plasma energy ($\omega \gg \omega_p$), the observed transitions correspond to single-particle interband excitations between Landau levels. Tracing their field-dependence may provide us with a useful insight into the electronic band structure of Cd_3As_2 . All excitations show a well-defined \sqrt{B} dependence, which is in general characteristic of massless charge carriers, nevertheless, with a well defined negative offset of about $-(35 \pm 10)$ meV (Fig. 3c). This is in contrast to the cyclotron energy in the quantum limit, which is also linear in \sqrt{B} , but without any offset.⁶

Let us first analyze these data in a simplified way, using the semiclassical Bohr-Sommerfeld quantization,^{30,31} which only considers the orbital motion of electrons and neglects their spin. In this picture, the density of states, and consequently, also the joint density of states, becomes modulated due to the quantized cyclotron motion of electrons. With an assumption of isotropic bands (reasonably well justified for Cd_3As_2 ⁶) the cyclotron orbits are characterized by the momenta $k = \sqrt{2eB(n + \gamma)}/\hbar$, where n is integer ($n \geq 1$) and γ is a factor related to the

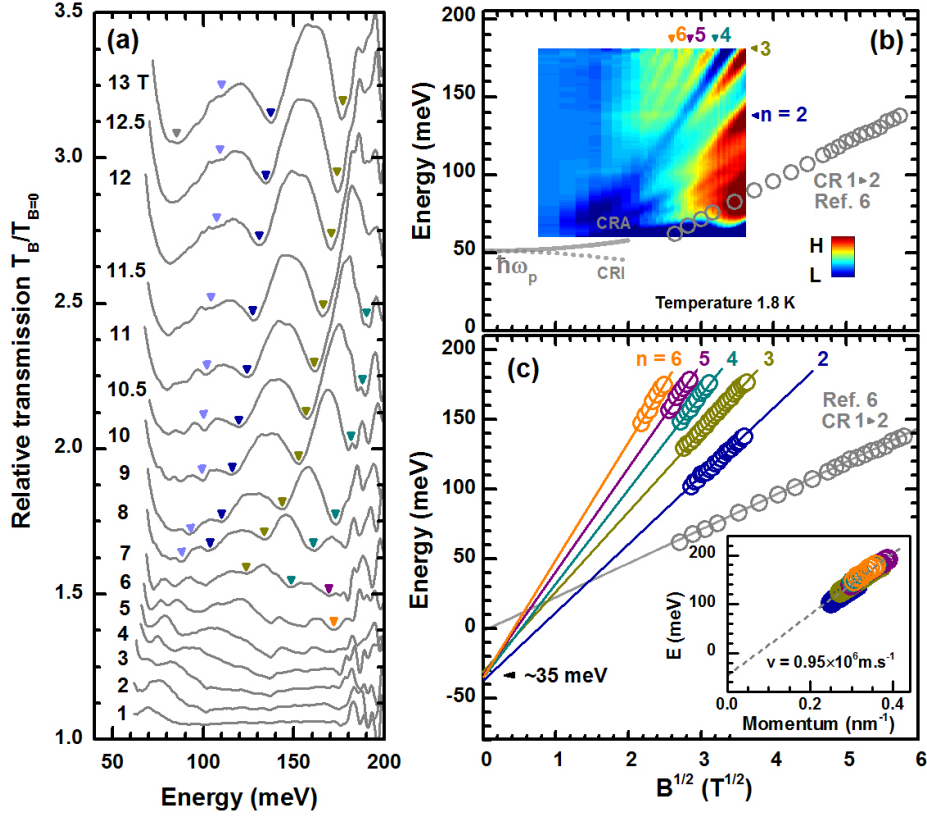


FIG. 3. (a) Relative magneto-transmission spectra $T_B/T_{B=0}$ of the explored Cd_3As_2 sample plotted for selected values of the magnetic field B applied. Individual inter-LL resonances are denoted by triangles. (b) The false color-map of magneto-absorbance spectra. The gray circles show the cyclotron energy (fundamental mode) obtained in the previous high-field magneto-reflectivity experiments⁶. (c) The experimentally extracted energies of inter-LL resonances versus \sqrt{B} . To exclude effects related to the coupling of interband (single-particle) excitations with plasmon (so-called Bernstein modes), only resonances at photon energies above $\hbar\omega = 100$ meV are plotted ($\hbar\omega_p \approx 50$ meV). The inset shows the linear energy-momentum dependence (the separation of the conduction and valence band) obtained using a simple semi-classical model based on the Bohr-Sommerfeld quantization, see the text.

Berry phase of the explored charge carriers ($0 \leq \gamma < 1$). This allows us to reconstruct the original band structure, *i.e.*, to get the energy distance from the valence to conduction band, from which the corresponding LLs are formed (the HH band and the upper cone).

Setting the indices n as specified in Fig. 3b,c ($n = 2, 3, 4, 5$ and 6), all experimental points reasonably well fall on a single line (inset of Fig. 3c), thus implying a nearly perfect linear energy-momentum dependence, with the slope reflecting the velocity parameter $v \approx 0.95 \times 10^6$ m/s. In the inset of Fig. 3c, we have considered, consistently with the Kane/Bodnar model, the phase factor $\gamma = 1/2$. Importantly, the deduced velocity exactly matches the value deduced for the upper conical conduction band in the original analysis of Bodnar,⁸ in the more recent STM/STS study⁵ as well as in cyclotron resonance experiment⁶. This remarkable agreement may only be explained by the existence of a nearly dispersionless valence band, from which electrons are promoted, via an optical excitation, to the conical conduction band (excitations from the blue to violet band in Fig. 1). This

is fully consistent with the Bodnar/Kane model⁹, which implies the existence of such a flat band. On the other hand, no flat band is expected in systems described by the Dirac Hamiltonian.

Now we analyze the negative offset of interband inter-LL excitations (seen in Fig. 3) in greater detail. Again, no such offset is expected for Dirac-type systems, with an exception for the unlikely case that the velocity parameter increases isotropically with momentum. This would imply strong parabolic corrections to the linear bands and thus equally strong deviations from the \sqrt{B} behavior of the magneto-optical transmission lines. The absence of such deviations precludes this type of band corrections as the origin of the negative offset. In contrast, the offset – either positive or negative – is expected in Kane semiconductors/semimetals with a non-zero band gap E_g , as visualized using the asymptotes in Fig. 4b. At photon energies larger than the band gap, $\hbar\omega \gg E_g$, the flat band becomes shifted with respect to the upper cone by $E_g/2$, which gives rise to the offset of the interband inter-LL excitations (when followed as a function of

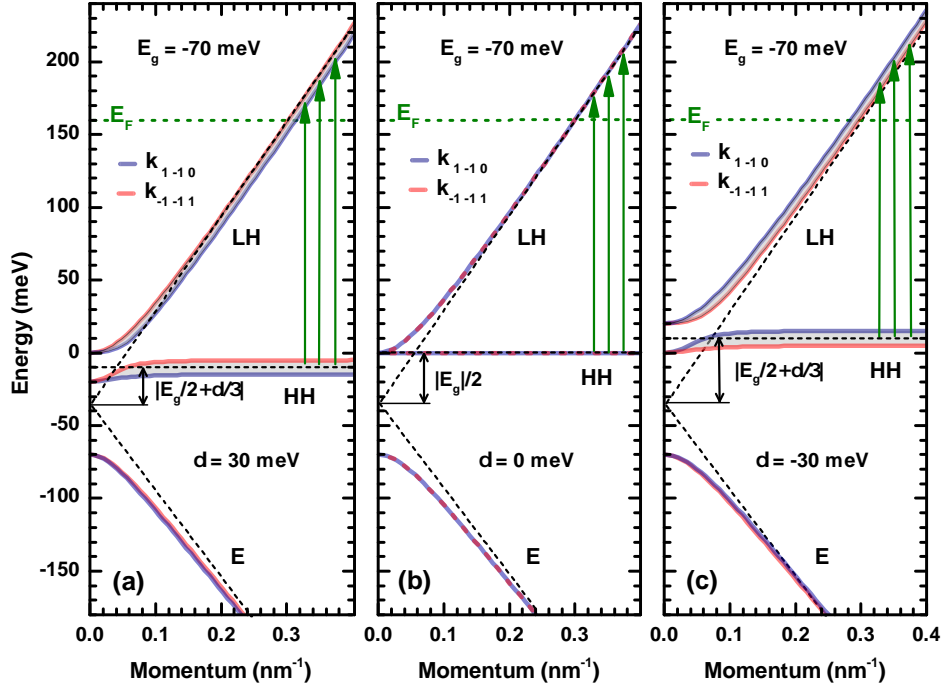


FIG. 4. The electronic band structure of Cd_3As_2 calculated within the Bodnar/Kane model for the fixed values of $E_g = -70$ meV and $v = 0.94 \times 10^6$ m/s, for three different strengths of crystal field splitting: $\delta = 30, 0$ and -30 meV, in parts (a), (b) and (c) respectively. The Dirac cones are expected to appear for positive δ , while for the negative one, the system should enter a topologically insulating phase. The electronic bands have been plotted along $(1 -1 0)$ and $(-1 -1 1)$ directions, which are perpendicular to the applied magnetic field, $B \parallel (112)$, as well as to each other. The non-zero δ parameter mainly impacts the HH band, which becomes modulated, anisotropic and shifted in energy by the average amount of $\delta/3$. As shown by the corresponding asymptotes, the upper cone thus becomes shifted with respect to the flat band, implying thus the offset of $E_g/2 + \delta/3$ for interband absorption (and interband inter-LL excitations in Fig. 3c). The vertical arrows denote interband excitations allowed by the occupation of the upper conical band, which dominantly contribute to interband absorption.

\sqrt{B}). The same conclusion can be drawn directly from the LL spectrum of Kane electrons. At photon energies significantly higher as compared to E_g , the energies of flat-to-upper-cone inter-LL transitions read (at $k = 0$): $E_g/2 + v\sqrt{2eB\hbar(n - 1/2 + \sigma)}$ for $n \geq 1$, where $\sigma = \pm 1/4$ stands for the spin projection, see Ref. 10 and related Supplementary materials.

When the full Bodnar model – with a non-zero crystal field splitting parameter δ – is considered, the situation becomes more complex and the band structure is no longer isotropic. This is best manifested by the modulation of the HH band, which is completely flat only for $\delta \equiv 0$. This modulation is illustrated in Figs. 4a,c, where the LH, HH and E bands have been plotted for two different crystallographic directions. These are perpendicular to the magnetic field applied along the $[112]$ direction and they were chosen to visualize the full width of the flat band induced by δ . For relatively small δ , the HH band remains fairly flat, but it is shifted by the average value of $\delta/3$. This implies an approximate offset of flat-to-cone inter-LL excitations: $E_g/2 + \delta/3$.

To estimate the E_g and δ parameters, the simplified analysis of our magneto-optical data based on the semiclassical Bohr-Sommerfeld model (see the inset of Fig. 3c)

has to be replaced with full quantum-mechanical treatment. To this end, we have numerically calculated the LL spectrum within the complete Bodnar model for the magnetic field oriented along the $[112]$ direction³², see Fig. 5. In these calculations, the velocity parameter was considered as isotropic and fixed at $v = 0.94 \times 10^6$ m/s, which is a value consistent with the original Bodnar's analysis⁸ as well as with more recent STM/STS and cyclotron resonance studies.^{5,6} The spin-orbit coupling, having rather weak influence on the resulting LL spectrum, was set as $\Delta = 400$ meV.⁶

The only tunable parameters in the calculations of the LL spectrum in Fig. 5 were thus the band gap E_g and the crystal-field splitting δ . We have considered their various combinations, with the approximate boundary condition implied by the offset $E_g/2 + \delta/3 \approx -35$ meV determined and discussed above. This is illustrated in Fig. 5, where our calculations are shown for (a): $E_g = -45$ meV, $\delta = -40$ meV, (b) $E_g = -70$ meV, $\delta = 0$ meV and (c) $E_g = -95$ meV, $\delta = 40$ meV, respectively. For electric-dipole-active excitations, which preserve spin and follow the selection rules $n \pm 1 \rightarrow n$,¹⁰ we obtain two transitions from the flat band into a given final-state LL with the index n_\uparrow or n_\downarrow , see Ref. 32 for more details.

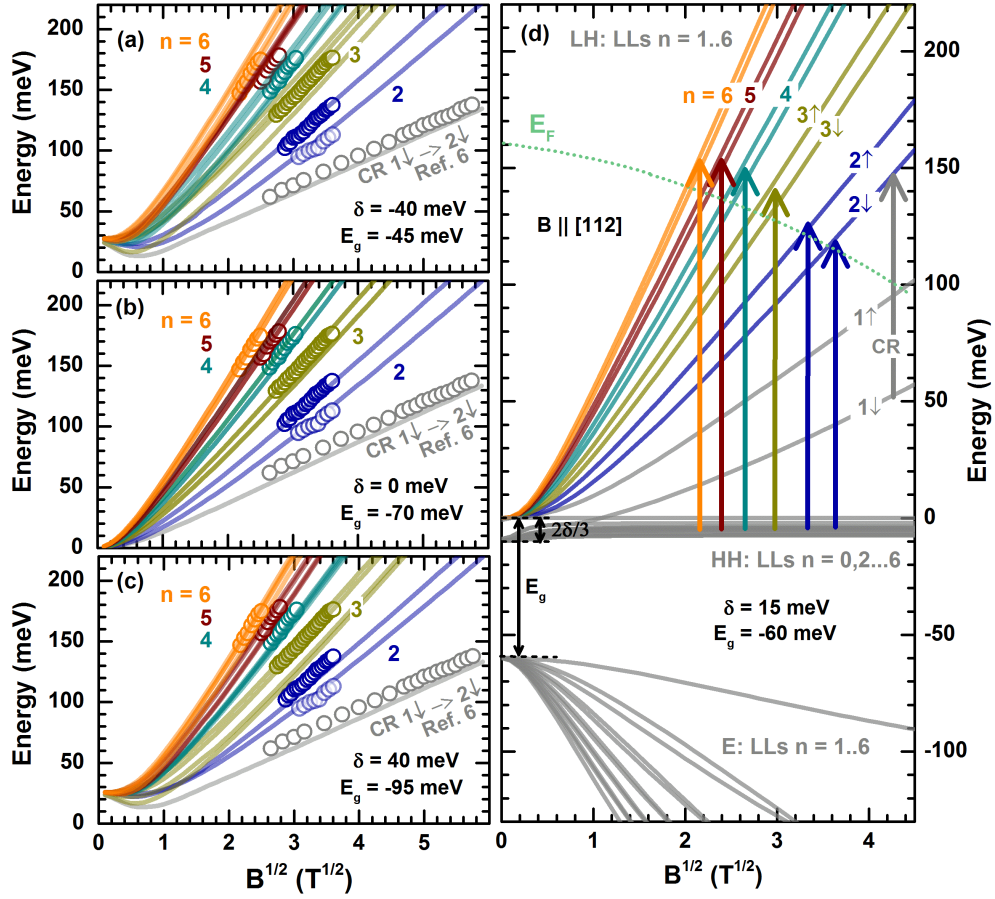


FIG. 5. Parts (a-c): The experimentally determined fan chart of observed inter-LL excitations compared to theoretically calculated excitation energies within the Bodnar (Kane) model for three different combinations of E_g and δ , which fulfill the condition $E_g/2 + \delta/3 \approx -35$ meV implied by the offset of interband excitations. The individual excitations are labeled by the corresponding final-state LL and also by particular color-coding in (d), where the field-dependence of the LL spectrum ($n = 0, 1, 2 \dots 6$), calculated for $E_g = -60$ meV and $\delta = 15$ meV, has been plotted. The velocity parameter was fixed at $v = 0.94 \times 10^6$ m/s and the strength of the spin-orbit coupling at $\Delta = 400$ meV. The model does not include any other free parameters. The CR data are taken from our previous magneto-reflectivity experiments.⁶ The dashed line in (d) denotes an approximate position of the Fermi energy as a function of B . In the parts (a-c), the lowest in energy interband transition (light blue) may be identified as the excitation from the flat band to 2_\downarrow level, but its energy also coincides with the intraband $1_\downarrow \rightarrow 3_\downarrow$ excitation, which may become electric-dipole-active due to the lack of full isotropy in the studied system.

Experimentally, the splitting of transitions due to spin is resolved only for the lowest final-state LL $n = 2$, cf., Fig. 5d.

The best agreement between the experimental data and theoretically expected energies of inter-LL excitations was found for $|\delta| \approx 0$, for which the Bodnar model reduces down to even more simple Kane model with an effectively vanishing energy scale of Dirac cones. For the crystal-field splitting as low as $|\delta| = 40$ meV, the departure of theoretical lines from experimental points becomes significant enough that it allows us to set, while being conservative in this estimate, the interval of acceptable values to $|\delta| < 40$ meV.

Let us recall that it is the sign of the δ parameter, which determines whether the system with an inverted band gap becomes a 3D Dirac semimetal (for $\delta > 0$) or a topological insulator (for $\delta < 0$). Clearly, our magneto-

optical data do not allow us to determine the sign of δ . Nevertheless, one may profit, in this case, from ab initio calculations of the Cd_3As_2 band structure presented, for instance, in Refs. 1, 2, 7, and 15. The absolute values of energy splitting and band gaps deduced theoretically may not be very accurate. On the other hand, the ordering of bands, which among other things implies the sign of δ , represents rather reliable output. The available theoretical works predict positive value of δ , see, e.g., Refs. 1 and 7. This allows us to reduce the interval of the expected crystal field splitting to $0 < \delta < 40$ meV.

As a matter of fact, it is the tetragonal lattice of Cd_3As_2 itself, with the out-of-plane lattice constant elongated with respect to the in-plane components ($c/2 > a = b$), which determines the sign of the δ parameter. In HgTe , which is another well-known Kane semimetal ($E_g = -300$ meV), lateral expansion of the lattice gives

rise to a negative crystal-field splitting ($\delta < 0$), and therefore, to a topological insulating phase, which has been extensively studied experimentally.^{35,36} In contrast, compressive lateral strain is expected to transform HgTe into a 3D symmetry-protected Dirac semimetal (with $\delta > 0$). Therefore, staying strictly with estimates based on our experimental magneto-optical data ($|\delta| < 40$ meV) only, one cannot unambiguously decide whether Cd₃As₂ is a symmetry-protected Dirac semimetal or a topological insulator with a very narrow band gap in bulk.

Let us also note that the negative sign of the band gap in Cd₃As₂ reflects an inverted ordering of bands in this system, and consequently, implies the appearance of surface states, similar to those in topological insulators.³⁷ Such surface states have already been observed in another inverted-gap Kane semimetal HgTe.³⁸ In Cd₃As₂, however, the situation might be more complex. The surface states, which appear due to the band inversion, might coexist with the Fermi arcs, which are predicted for this material due to the presence of a pair of Dirac nodes (two pairs of Weyl nodes) at low energies. At present, our magneto-optical data do not provide us with any clear signature of surface states, but their presence was discussed in the context of ARPES and magneto-transport experiments.^{39–41}

III. CONCLUSIONS

In summary, we have performed magneto-transmission experiments on Cd₃As₂. The observed magneto-optical

response, comprising a series of interband inter-Landau level excitations, allow us to determine the band structure parameters relevant for the scale and shape of possibly present Dirac cones in this material. The estimated crystal field splitting, $0 < \delta < 40$ meV, represents the very upper limit for the energy of Dirac electrons in Cd₃As₂. These relativistic-like particles thus may emerge in the band structure only at energies far below the Fermi level, which in available samples typically exceeds 100 meV (in our case $E_F \approx 160$ meV). At energies significantly higher than δ , the system behaves as an ordinary Kane semimetal^{6,9,13,42} characterized by a small inverted band gap of $E_g = (-70 \pm 20)$ meV.

Acknowledgements

This work was supported by ERC MOMB (No. 320590), TWINFUSYON (No. 692034), Lia TeraMIR, TERASENS, by MEYS CEITEC 2020 (No. LQ1601) and by ANR DIRAC3D projects and MoST-CNRS exchange programme (DIRAC3D). We acknowledge the support of LNCMI-CNRS, a member of the European Magnetic Field Laboratory (EMFL). The authors also acknowledge discussions with D. M. Basko, A. O. Slobodeniuk and N. Miller. A. A. acknowledges funding from The Ambizione Fellowship of the Swiss National Science Foundation. I. C. acknowledges support from the post-doc mobility programme of the Swiss NSF.

* michaelhaki@email.cz

† milan.orlita@lncmi.cnrs.fr

¹ Z. Wang, H. Weng, Q. Wu, X. Dai, and Z. Fang, *Phys. Rev. B* **88**, 125427 (2013).

² S. Borisenko, Q. Gibson, D. Evtushinsky, V. Zabolotnyy, B. Büchner, and R. J. Cava, *Phys. Rev. Lett.* **113**, 027603 (2014).

³ M. Neupane, S.-Y. Xu, R. Sankar, N. Alidoust, G. Bian, C. Liu, I. Belopolski, T.-R. Chang, H.-T. Jeng, H. Lin, *et al.*, *Nature Comm.* **5**, 3786 (2014).

⁴ Z. K. Liu, B. Zhou, Y. Zhang, Z. J. Wang, H. M. Weng, D. Prabhakaran, S.-K. Mo, Z. X. Shen, Z. Fang, X. Dai, Z. Hussain, and Y. L. Chen, *Science* **343**, 864 (2014).

⁵ S. Jeon, B. B. Zhou, A. Gyenis, B. E. Feldman, I. Kimchi, A. C. Potter, Q. D. Gibson, R. J. Cava, A. Vishwanath, and A. Yazdani, *Nature Mater.* **13**, 851 (2014).

⁶ A. Akrap, M. Hakl, S. Tchoumakov, I. Crassee, J. Kuba, M. O. Goerbig, C. C. Homes, and *et al.*, *Phys. Rev. Lett.* **117**, 136401 (2016).

⁷ A. M. Conte, O. Pulci, and F. Bechstedt, *Sci. Rep.* **7**, 45500 (2017).

⁸ J. Bodnar, in *Proc. III Conf. Narrow-Gap Semiconductors, Warsaw*, edited by J. Rauhuszkiwicz, M. Górska, and E. Kaczmarek (Elsevier, 1977) p. 311.

⁹ E. O. Kane, *J. Phys. Chem. Solids* **1**, 249 (1957).

¹⁰ M. Orlita, D. M. Basko, M. S. Zholudev, F. Teppe, W. Knap, V. I. Gavrilenco, N. N. Mikhailov, S. A. Dvoretiskii, P. Neugebauer, C. Faugeras, *et al.*, *Nature Phys.* **10**, 233 (2014).

¹¹ F. Teppe, M. Marcinkiewicz, S. S. Krishtopenko, S. Ruffenach, C. Consejo, A. M. Kadykov, W. Desrat, D. But, W. Knap, J. Ludwig, S. Moon, D. Smirnov, M. Orlita, Z. Jiang, S. V. Morozov, V. I. Gavrilenco, N. N. Mikhailov, and S. A. Dvoretiskii, *Nature Commun.* **7**, 12576 (2016).

¹² H. Kildal, *Phys. Rev. B* **10**, 5082 (1974).

¹³ P. Y. Yu and M. Cardona, *Fundamentals of Semiconductors* (Springer, Berlin Heidelberg, 2010).

¹⁴ A. Rambo and M. J. Aubin, *Can. J. Phys.* **57**, 2093 (1979).

¹⁵ M. N. Ali, Q. Gibson, S. Jeon, B. B. Zhou, A. Yazdani, and R. J. Cava, *Inorganic Chemistry* **53**, 4062 (2014).

¹⁶ I. Rosenman, *J. Phys. Chem. Solids* **30**, 1385 (1969).

¹⁷ W. Zdanowicz, L. Zdanowicz, J. Portal, and S. Askenazy, *Thin Solid Films* **61**, 41 (1979).

¹⁸ E. Arushanov, *Prog. Cryst. Growth Ch.* **3**, 211 (1980).

¹⁹ E. Arushanov, *Prog. Cryst. Growth Ch.* **25**, 131 (1992).

²⁰ M. Gelten, C. van Es, F. Blom, and J. Jongeneelen, *Solid State Commun.* **33**, 833 (1980).

²¹ D. Neubauer *et al.*, *Phys. Rev. B* **93**, 121202 (2016).

²² I. Crassee, E. Martino, C. C. Homes, O. Caha, J. Novak, P. Tuckmantel, M. Hakl, A. Nateprov, E. Arushanov,

- Q. Gibbson, R. Cava, S. Koohpayeh, K. Arpino, T. McQueen, M. Orlita, and A. Akrap, [arxiv:1712.03147](#).
- ²³ T. Timusk, J. P. Carbotte, C. C. Homes, D. N. Basov, and S. G. Sharapov, *Phys. Rev. B* **87**, 235121 (2013).
 - ²⁴ I. B. Bernstein, *Phys. Rev.* **109**, 10 (1958).
 - ²⁵ E. Batke, D. Heitmann, and C. W. Tu, *Phys. Rev. B* **34**, 6951 (1986).
 - ²⁶ E. Batke, D. Heitmann, J. P. Kotthaus, and K. Ploog, *Phys. Rev. Lett.* **54**, 2367 (1985).
 - ²⁷ A. Wysmolek, D. Plantier, M. Potemski, T. Shupinski, and Z. R. Żytkiewicz, *Phys. Rev. B* **74**, 165206 (2006).
 - ²⁸ R. Roldán, M. O. Goerbig, and J.-N. Fuchs, *Phys. Rev. B* **83**, 205406 (2011).
 - ²⁹ E. D. Palik and J. Furdyna, *Rep. Prog. Phys.* **33**, 1193 (1970).
 - ³⁰ L. Onsager, *Philos. Mag.* **43**, 1006 (1952).
 - ³¹ M. O. Goerbig, G. Montambaux, and F. Pichon, *EPL (Europhysics Letters)* **105**, 57005 (2014).
 - ³² See Supplementary materials, which include Refs. 33 and 34, for details about theoretical model and data analysis.
 - ³³ P. R. Wallace, *phys. stat. sol. (b)* **92**, 49 (1979).
 - ³⁴ M. Orlita, P. Neugebauer, C. Faugeras, A.-L. Barra, M. Potemski, F. M. D. Pellegrino, and D. M. Basko, *Phys. Rev. Lett.* **108**, 017602 (2012).
 - ³⁵ C. Brüne, C. X. Liu, E. G. Novik, E. M. Hankiewicz, H. Buhmann, Y. L. Chen, X. L. Qi, Z. X. Shen, S. C. Zhang, and L. W. Molenkamp, *Phys. Rev. Lett.* **106**, 126803 (2011).
 - ³⁶ V. Dziom, A. Shuvaev, A. Pimenov, G. V. Astakhov, C. Ames, K. Bendias, J. Böttcher, G. Tkachov, E. M. Hankiewicz, C. Brüne, *et al.*, *Nature Commun.* **8**, 15197 (2017).
 - ³⁷ M. Z. Hasan and C. L. Kane, *Rev. Mod. Phys.* **82**, 3045 (2010).
 - ³⁸ C. Liu, G. Bian, T.-R. Chang, K. Wang, S.-Y. Xu, I. Belopolski, I. Miotkowski, H. Cao, K. Miyamoto, C. Xu, C. E. Matt, T. Schmitt, N. Alidoust, M. Neupane, H.-T. Jeng, H. Lin, A. Bansil, V. N. Strocov, M. Bissen, A. V. Fedorov, X. Xiao, T. Okuda, Y. P. Chen, and M. Z. Hasan, *Phys. Rev. B* **92**, 115436 (2015).
 - ³⁹ H. Yi, Z. Wang, C. Chen, Y. Shi, Y. Feng, A. Liang, Z. Xie, S. He, J. He, Y. Peng, X. Liu, Y. Liu, L. Zhao, G. Liu, X. Dong, J. Zhang, M. Nakatake, M. Arita, K. Shimada, H. Namatame, M. Taniguchi, Z. Xu, C. Chen, X. Dai, Z. Fang, and X. J. Zhou, *Sci. Rep.* **4** (2014), [10.1038/srep06106](#).
 - ⁴⁰ C. Zhang, A. Narayan, S. Lu, J. Zhang, H. Zhang, Z. Ni, X. Yuan, Y. Liu, J.-H. Park, E. Zhang, *et al.*, *Nature Communications* **8**, 1272 (2017).
 - ⁴¹ T. Schumann, L. Galletti, D. A. Kealhofer, H. Kim, M. Goyal, and S. Stemmer, *Phys. Rev. Lett.* **120**, 016801 (2018).
 - ⁴² P. Kacman and W. Zawadzki, *phys. stat. sol. (b)* **47**, 629 (1971).

Supplementary Materials for “The energy scale of Dirac electrons in Cd₃As₂”

M. Haki,^{1,*} S. Tchoumakov,² I. Crassee,¹ A. Akrap,³ B. A. Piot,¹ C. Faugeras,¹
 G. Martinez,¹ A. Nateprov,⁴ E. Arushanov,⁴ F. Teppe,⁵ R. Sankar,^{6,7} Wei-li Lee,⁶
 J. Debray,^{8,9} O. Caha,¹⁰ J. Novák,¹⁰ M. O. Goerbig,² M. Potemski,¹ and M. Orlita^{1,11,†}

¹*Laboratoire National des Champs Magnétiques Intenses,
 CNRS-UGA-UPS-INSa, 25, avenue des Martyrs, 38042 Grenoble, France*

²*LPS, Univ. Paris-Sud, Univ. Paris-Saclay, CNRS UMR 8502, 91405 Orsay, France*

³*DQMP, University of Geneva, 1211 Geneva 4, Switzerland*

⁴*Institute of Applied Physics, Academy of Sciences of Moldova, 2028 Chisinau, Moldova*

⁵*Laboratoire Charles Coulomb, CNRS, Université Montpellier, 34095 Montpellier, France*

⁶*Institute of Physics, Academia Sinica, Nankang, 11529 Taipei, Taiwan*

⁷*Center for Condensed Matter Sciences, National Taiwan University, Taipei 10617, Taiwan*

⁸*Université Grenoble Alpes, Institut NEEL, F-38000 Grenoble, France*

⁹*CNRS, Institut NEEL, F-38000 Grenoble, France*

¹⁰*CEITEC MU and Faculty of Science, Masaryk University, 61137 Brno, Czech Republic*

¹¹*Institute of Physics, Charles University, Ke Karlovu 5, 12116 Praha 2, Czech Republic*

In these Supplementary Materials, we provide details about calculations of the Landau level spectrum within the Bodnar model, assuming that the magnetic field B is oriented along the (112) crystallographic direction. We also present a comparison of our experimental data with expectations of the simple Kane model, which completely neglects the influence of the crystal-field splitting parameter δ .

LANDAU LEVEL QUANTIZATION FOR (112)-ORIENTATED BODNAR HAMILTONIAN

Due to the anisotropy of the electronic band structure implied by the Bodnar model, which is best visible at relatively low energies and which is closely related to the possible appearance of Dirac cones, the corresponding Landau level spectrum depends on the particular orientation of the applied magnetic field. The simplest case, with B oriented along the tetragonal (001) axis was reviewed in the context of our preceding cyclotron resonance study [1]. Here we present calculations for the magnetic field oriented along the (112) direction, which is the natural direction of Cd₃As₂ growth/cleavage and which is also relevant for the magneto-transmission experiment presented in the main part of this work. Let us also note that the (112) direction within the full unit cell of Cd₃As₂ corresponds to the (111) direction within the simplifying anti-fluorite lattice considered by Bodnar [2].

In the magnetic field, which is applied along a generally oriented unit vector $(\sin \theta, 0, \cos \theta)^T$, the commutation relations satisfy:

$$[k_x, k_y] = -\frac{i}{l_B^2} \cos \theta, [k_x, k_z] = 0, [k_y, k_z] = -\frac{i}{l_B^2} \sin \theta. \quad (1)$$

Using these commutation relations in the Bodnar model [3], the Landau level spectrum may be calculated from the implicit equation:

$$\gamma(E_n) = \frac{\text{sgn} f_1(E_n)(2n+1)}{l_B^2} \sqrt{f_1(E_n)(\cos^2 \theta f_1(E_n) + \sin^2 \theta f_2(E_n))} \\ + \frac{f_1(E_n) f_2 E_n}{\cos^2 \theta f_1(E_n) + \sin^2 \theta f_2(E_n)} k_z^2 \pm \frac{P_\perp \Delta}{3l_B^2} \sqrt{(E_n + \delta)^2 P_\perp^2 \cos^2 \theta + E_n^2 P_\parallel^2 \sin^2 \theta} \quad (2)$$

where the auxiliary functions γ, f_1, f_2 are defined as

$$\gamma(E) = E(E - E_g)[E(E + \Delta) + \delta(E + \frac{2}{3}\Delta)], \\ f_1(E) = P_\perp^2 [E(E + \frac{2}{3}\Delta) + \delta(E + \frac{1}{3}\Delta)], \\ f_2(E) = P_\parallel^2 E(E + \frac{2}{3}\Delta) \quad (3)$$

and where the anisotropic Kane parameters, P_\perp and P_\parallel are related to the (anisotropic) velocity parameter as $v_{\perp,\parallel} = \sqrt{\frac{2}{3}} P_{\perp,\parallel} / \hbar$. The signs (+) and (-) refer to the spin set up and down, respectively. The above equation is valid

outside the interval of energies $-\tan^2 \theta < f_1(E_n)/f_2(E_n) < 0$ that covers the region of the heavy-hole band for $\delta > 0$. The corresponding eigenfunctions take the standard form $\Psi = (\psi_j)_{j=1..8}$ where each component $\psi_j = a_j |n\rangle_j u_j$ is expressed just by a single harmonic function $|n\rangle_j$ and a basis vector u_j .

Another possible approach is to rotate the whole Bodnar Hamiltonian into a new coordination system, in which the z -axis coincides with the direction of the applied magnetic field: $\mathbf{B} = (0, 0, B)^\top$. This can be done by rescaling and rotation of the momentum coordinates q_x, q_y, q_z through the following transformation:

$$\begin{pmatrix} q_x \\ q_y \\ q_z \end{pmatrix} = \begin{pmatrix} \frac{P_\perp}{P} \cos \xi & 0 & -\frac{P_\parallel}{P} \sin \xi \\ 0 & \frac{P_\perp}{P} & 0 \\ \frac{P_\perp}{P} \sin \xi & 0 & \frac{P_\parallel}{P} \cos \xi \end{pmatrix} \begin{pmatrix} k_x \\ k_y \\ k_z \end{pmatrix}. \quad (4)$$

The new commutation relations then take the form:

$$[q_x, q_y] = -\frac{i}{l_B^2} \left(\frac{P_\perp^2 \cos(\xi) \cos(\theta) + P_\perp P_\parallel \sin(\xi) \sin(\theta)}{P^2} \right), \quad [q_x, q_z] = 0, \quad [q_y, q_z] = \frac{i}{l_B^2} \frac{P_\perp}{P} \left[\frac{P_\perp}{P} \cos(\theta) \sin(\xi) - \frac{P_\parallel}{P} \cos(\xi) \sin(\theta) \right]. \quad (5)$$

which we simplify choosing ξ and P such that

$$P = \sqrt{|P_\perp^2 \cos(\xi) \cos(\theta) + P_\perp P_\parallel \sin(\xi) \sin(\theta)|}, \quad (6)$$

$$\xi = \arctan \left[\frac{P_\perp}{P_\parallel} \tan(\theta) \right]. \quad (7)$$

This way one finds

$$[q_x, q_y] = -\frac{i}{l_B^2}, \quad [q_x, q_z] = 0, \quad [q_y, q_z] = 0. \quad (8)$$

The corresponding Hamiltonian undergoes a unitary transformation $\hat{H}_\xi = U_\xi^{-1} \hat{H} U_\xi$ and reads (in its matrix form):

$$\begin{pmatrix} E_g & Pq_- & -Pq_+ & 0 & 0 & 0 & 0 & Pq_z \\ Pq_+ & -\frac{\delta \sin^2(\xi)}{2} & \frac{\delta \sin^2(\xi)}{2} & 0 & 0 & 0 & 0 & \frac{\delta \sin(2\xi)}{2\sqrt{2}} \\ -Pq_- & \frac{\delta \sin^2(\xi)}{2} & -\frac{\delta \sin^2(\xi)}{2} - \frac{2}{3}\Delta & \frac{\sqrt{2}\Delta}{3} & 0 & 0 & 0 & -\frac{\delta \sin(2\xi)}{2\sqrt{2}} \\ 0 & 0 & \frac{\sqrt{2}\Delta}{3} & -\delta \cos^2(\xi) - \frac{\Delta}{3} & Pq_z & \frac{\delta \sin(2\xi)}{2\sqrt{2}} & \frac{\delta \sin(2\xi)}{2\sqrt{2}} & 0 \\ 0 & 0 & 0 & Pq_z & E_g & Pq_+ & Pq_- & 0 \\ 0 & 0 & 0 & \frac{\delta \sin(2\xi)}{2\sqrt{2}} & Pq_- & -\frac{\delta \sin^2(\xi)}{2} & -\frac{\delta \sin^2(\xi)}{2} & 0 \\ 0 & 0 & 0 & \frac{\delta \sin(2\xi)}{2\sqrt{2}} & Pq_+ & -\frac{\delta \sin^2(\xi)}{2} & -\frac{\delta \sin^2(\xi)}{2} - \frac{2}{3}\Delta & \frac{\sqrt{2}\Delta}{3} \\ Pq_z & \frac{\delta \sin(2\xi)}{2\sqrt{2}} & -\frac{\delta \sin(2\xi)}{2\sqrt{2}} & 0 & 0 & 0 & \frac{\sqrt{2}\Delta}{3} & -\delta \cos^2(\xi) - \frac{\Delta}{3} \end{pmatrix} \quad (9)$$

with the corresponding LS-basis:

$$(s \uparrow, u_{-1} \uparrow, u_0 \uparrow, u_{+1} \uparrow, s \downarrow, u_{-1} \downarrow, u_0 \downarrow, u_{+1} \downarrow), \quad (10)$$

where u_n functions are built for $L = 1$ as:

$$u_{-1} = \frac{i}{\sqrt{2}}(u_x - iu_y), \quad u_0 = iu_z, \quad u_1 = \frac{-i}{\sqrt{2}}(u_x + iu_y). \quad (11)$$

When we introduce the magnetic field into the above Hamiltonian, via standard ladder operators, one may conclude that no simple eight-component vector can satisfy all ladder operations in the eigenproblem $H_{(112)}\Psi = E\Psi$ at once and a more general ansatz, using a perturbative approach for the each component of the wavefunction $\Psi = (\psi_j)_{j=1..8}$, needs to be chosen:

$$\psi_j = \sum_{n=0}^{N_{\max}} a_{j,n} |n\rangle, \quad (12)$$

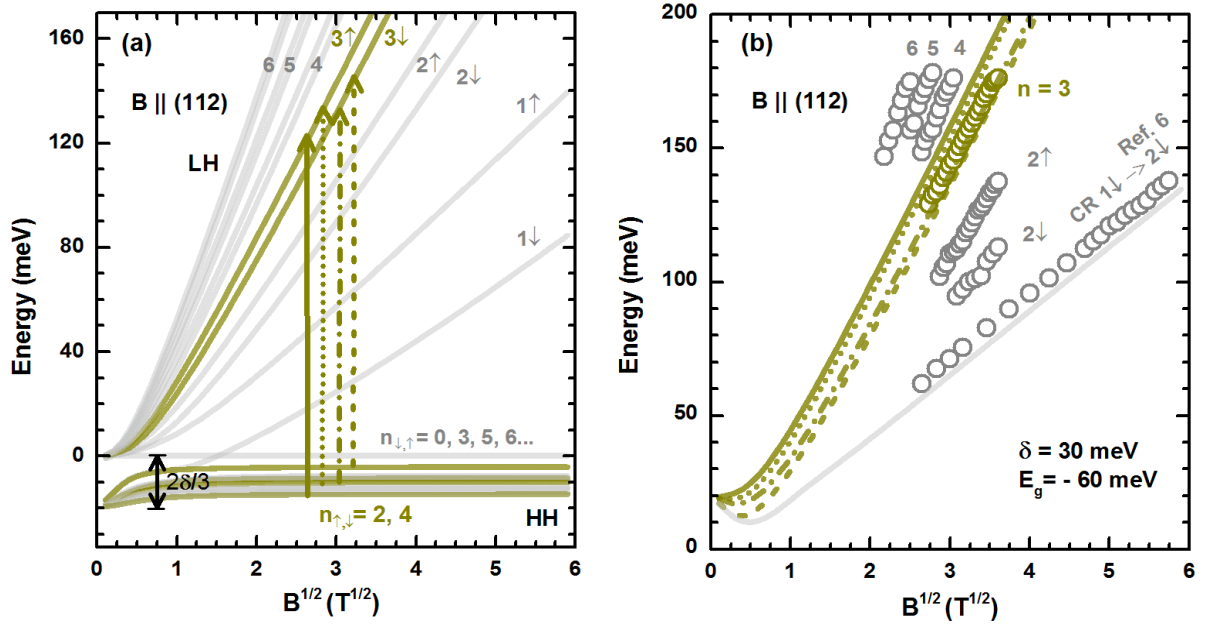


FIG. 1. (a) Landau level spectrum calculated within the Bodnar model for $E_g = -60$ meV and $\delta = 30$ meV with the magnetic field oriented along the (112) direction. The vertical arrows denote the quadruplet of inter-Landau level transitions from the flat band to the upper conical band with the final-state level $n = 3$. (b) the experimental position of observed resonances compared to the theoretically expected transition energies calculated from (a).

where N_{\max} stands for the order of the expansion. Using this ansatz, we finally end up with the following set of eight equations:

$$\sum_{j=1}^8 \sum_{n=0}^{N_{\max}} H_{ij} a_{j,n} |n\rangle = E \sum_{n=0}^{N_{\max}} a_{j,n} |n\rangle. \quad (13)$$

When each equation is projected out by one of the harmonic function $\langle n' |_{n'=1 \dots N_{\max}}$ in the solution (12), the coefficients $a_{j,n}$ can be obtained as:

$$\sum_{j=1}^8 \sum_{n=0}^{N_{\max}} \langle n' | H_{ij} | n \rangle a_{j,n} = E \sum_{n=0}^{N_{\max}} a_{j,n} \delta_{n',n}. \quad (14)$$

Altogether, the set of $N_{\max} \times 8$ equations (14) provides us with the energies of N_{\max} Landau levels for each from the eight bands.

COMPARING THEORETICAL ENERGIES OF INTER-LANDAU LEVEL EXCITATIONS WITH EXPERIMENTS

Having calculated the Landau level spectrum, we may compare the expected energies of inter-Landau level excitations with positions of excitations identified experimentally. In this comparison (see Fig. 5 in the main text), we have considered the standard $n \pm 1 \rightarrow n$ selection rules, typical of electric-dipole active excitations in systems with an isotropic band structure. Strictly speaking, one may expect a richer excitation spectrum in systems with an anisotropic band structure, implying an additional set of electric-dipole-active excitations, which go beyond these simple selection rules. This fact may be illustrated, for instance, on the complex cyclotron resonance response of K point electrons in bulk graphite, which is characterized by a strongly anisotropic Fermi surface [4]. In the case of Cd_3As_2 , however, the anisotropy of the electronic band structure is relatively weak [1, 2], and therefore, one may expect that the transitions following the $n \pm 1 \rightarrow n$ selection rules dominate the magneto-optical response.

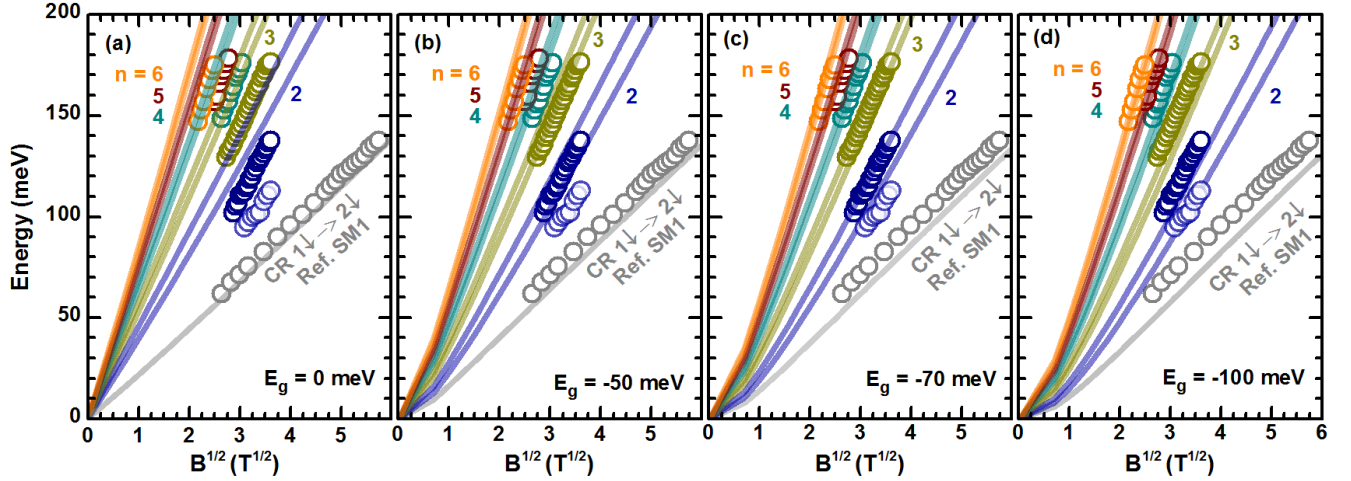


FIG. 2. A comparison of experimental data with theoretically expected positions of resonances calculated within the Kane model ($\delta = 0$) for several values of the (inverted) band gap $E_g = 0, -50, -70$ and -100 meV. The color coding is the same as in Fig. 5 of the main text. The best agreement is found for the band gap around $E_g \approx -70$ meV, which allows us to reproduce the experimental data for both, cyclotron resonance response [1] and interband inter-Landau level resonances, with a reasonable precision.

Staying with the $n \pm 1 \rightarrow n$ selections and focusing on excitations relevant for our experiment – from the flat band to the upper conical band – we get a pair of excitations into each final-state Landau level in the conduction band with a given spin projection $n_{\uparrow, \downarrow}$. For each Landau level index n , we thus get altogether four excitations from the flat band to the upper conical band: due to spin splitting of levels in the conduction band and due to the degeneracy of the flat band, which is removed by a non-zero crystal field splitting parameter δ . We illustrate this in Fig. S1 for the case of excitations with the final state in the Landau level $n = 3$. An exemption appears only for the final-state $n = 2$ level, for which only a single pair of excitations: $3\uparrow \rightarrow 2\uparrow$ and $3\downarrow \rightarrow 2\downarrow$, emerges. This is because the $n = 1$ levels are completely missing in the spectrum of the flat band [5].

In the main text, we compare the theoretically calculated excitation energies with our experimental data. All four transitions for each final-state LL $n = 3, 4, 5$ and 6 and two for $n = 2$ have been plotted in Figs. 5a-c. The corresponding color coding facilitates the association of the theoretical lines with the experimental points (see Fig. 5d of the main text). We conclude that the only for $n = 2$ final-state level clear splitting of lines is observed. For $n > 2$, the quadruples of excitations seems to be smeared due to finite widths of individual line. The absence of splitting may be considered as another indication of relatively small δ parameter in Cd_3As_2 .

Having concluded small crystal field splitting parameter δ , we may finish our discussion by the comparison of our experimental data with predictions of the (gapped) Kane model. In this case, it is the band gap E_g , which remains to be the only tunable parameter, since the velocity parameter is fixed at the value of $v = 0.94 \times 10^6$ m/s known from preceding experimental studies [1, 2, 6]. The theoretically expected energies of inter-Landau level excitations for four different values of the band gap: $E_g = 0, -50, -70$ and -100 meV, have been plotted in Figs. 2a-d and directly compared to the experimental data. Clearly, good agreement is achieved for the band gap values close to -70 meV. As one may expect, those are interband excitations which are more sensitive to E_g . Interestingly, the band gap value of $E_g = -70$ meV represents a certain trade-off, which compromises the agreement of the theoretical lines with the intraband (cyclotron resonance) data [1] and interband excitations (from magneto-transmission experiments presented in this work).

* michaelhakl@email.cz

† milan.orlita@lncmi.cnrs.fr

- [1] A. Akrap, M. Hakl, S. Tchoumakov, I. Crassee, J. Kuba, M. O. Goerbig, C. C. Homes, and et al. Magneto-optical signature of massless Kane electrons in cd_3as_2 . *Phys. Rev. Lett.*, 117:136401, 2016.
- [2] J. Bodnar. Band structure of cd_3as_2 from shibnikov-de hass and de hass-alphen effects. In J. Rauhuzkiewicz, M. Górka, and E. Kaczmarek, editors, *Proc. III Conf. Narrow-Gap Semiconductors, Warsaw*, page 311. Elsevier, 1977.

- [3] P. R. Wallace. Electronic g-factor in Cd_3As_2 . *Physica Status Solidi (b)*, 92(1):49–55, 1979.
- [4] M. Orlita, P. Neugebauer, C. Faugeras, A.-L. Barra, M. Potemski, F. M. D. Pellegrino, and D. M. Basko. Cyclotron motion in the vicinity of a lifshitz transition in graphite. *Phys. Rev. Lett.*, 108:017602, Jan 2012.
- [5] M. Orlita, D. M. Basko, M. S. Zholudev, F. Teppe, W. Knap, V. I. Gavrilenko, N. N. Mikhailov, S. A. Dvoretiskii, P. Neugebauer, C. Faugeras, A.-L. Barra, G. Martinez, and M. Potemski. Observation of three-dimensional massless kane fermions in a zinc-blende crystal. *Nature Phys.*, 10:233, 2014.
- [6] Sangjun Jeon et al. Landau quantization and quasiparticle interference in the three-dimensional dirac semimetal cd_3as_2 . *Nature Mater.*, 13:851–856, 2014.